Computational modeling of solid tumor evolution via a general Cartesian mesh/level set method

Cosmina S. Hogea[a], Bruce T. Murray[a], James A. Sethian[b]

[a]Department of Mechanical Engineering, Binghamton University, Binghamton, NY 13902, USA

[b]Department of Mathematics and Lawrence Berkeley National Laboratory, University of California, Berkeley, CA 94721, USA

Abstract

A computational framework for simulating tumor evolution based on continuum models is proposed. The advantages of the methodology are generality and relative simplicity of implementation. The Cartesian mesh/level set method developed here provides a computational tool for the investigation of a host of PDE-based tumor growth models, that may exhibit complicated tumor boundary evolution. Moreover, extending the approach to three-dimensional simulations is straightforward from an algorithmic perspective. The methodology is tested on a simplified tumor growth model with a numerical implementation in two dimensions; comparisons with results obtained from a linear analysis of the model and with published boundary integral simulations show good agreement.

1. Introduction

Over the last thirty years, research in several disciplines has led to the development of mathematical models to simulate the growth and macroscopic behavior of solid malignant tumors [16, 22]. A continuum-based model may be used to help predict the evolution of tumors in time and this knowledge would in turn help estimate the effect that various methods of treatment (e.g., chemotherapy, radiotherapy, laser radiation) would have on the tumor behavior as well as on the surrounding healthy tissue and, ultimately, on the host.

Malignant solid tumors generally are described as masses of tissue formed as a result of abnormal and excessive proliferation of mutant (atypical) cells, whose division has escaped the mechanisms that control normal cellular proliferation. This abnormal proliferation of atypical cells in time leads to an uncontrolled growth, extending to the adjacent surrounding tissues, infiltrating and invading them; this invasion is local at first–causing primary tumors, but malignant cells have the ability of migrating through the blood vessels and/or the lymphatic system towards other parts of the body, giving rise to secondary tumors; this process is called metastasis and it is the one responsible for the host death.

There are different stages of a malignant tumor evolution; described roughly, the main stages are the cellular stage and the macroscopic stage. The cellular stage refers to the early stage of a tumor evolution, when tumor cells are not condensed yet in a macroscopically observable mass. The macroscopic stage corresponds to that phase of a tumor evolution when clusters of atypical (malignant) cells condense together into a quasi-spherical observable mass (nucleus); this stage is sub-divided into two subsequent phases-the avascular phase and the vascular phase. During the avascular phase, the tumor obtains nutrients and "feeds" itself via diffusion processes alone, with nutrients already existing in the environment. In the second phase, called the vascular phase, when the tumor grows more rapidly through what is called angiogenesis (i.e., the birth of new blood vessels), malignant tumor cells secrete chemicals that have the ability to diffuse into the surrounding healthy tissues and stimulate the growth of new capillary blood vessels; the newly born blood vessels penetrate into the tumor mass feeding it with nutrients and leading to a rapid growth of the tumor. Tumor growth (spread of malignant cells) occurs basically via two mechanisms: when fed with a sufficient amount of nutrient, malignant cells divide (cellular mitosis); when the density of malignant cells in a specific volume becomes too high, the cells are compressed by their neighbors, so they tend to move to less compressed areas–where they are allowed to continue the division process–and this process is repeated.

Due to the extremely complex nature of the biological systems underlying the behavior in tumors and to the limited understanding of tumor growth mechanisms, developing useful models (mathematical, computational or both) is a difficult task. Currently, there are two major approaches in solid tumor growth modeling: one is via a "continuum model" that describes the evolution of the tumor in terms of systems of partial differential equations and/or non-linear integro-differential equations; the second is via a "discrete approach" employing cellular automata (CA) or lattice-based models. For the macroscopic stage of tumor evolution, the continuum approach may offer the most generality. Providing all of the model parameters can be estimated, the advantage of a continuum model is that it provides a systematic means for evaluating the role played by individual physical mechanisms.. However, the more complex the continuum model–the more difficult the computational simulations, since a continuum model will generally yield a nonlinear moving boundary problem described by systems of partial differential equations. The starting point for many continuum models is the pioneering work of Greenspan in the 1970's (see [22] and references therein). In recent years a variety of macroscopic continuum models have been derived employing analogies with inorganic systems (theory of mixtures, multiphase flow [18, 19]). While currently quite a few such complex models exist in the literature, computational simulations in arbitrary geometries and higher dimensions to further investigate and validate these models are still largely missing.

The goal of the present work is to introduce a general computational framework for obtaining multi-dimensional solutions to continuum-based models for numerically simulating tumor growth. The methodology is appropriate for complex models involving coupled nonlinear PDEs with moving boundaries in multi-phase domains. A fixed Cartesian grid is used to discretize the field equations–which allows good flexibility in the numerical implementation–coupled with a level set method to capture the moving tumor boundary. Various level set implementations have been successfully employed in

simulating a broad range of moving boundary problems in fluid mechanics, combustion, materials science, geophysics and computer vision. It seems natural to extend their application to moving boundary problems in biological applications.

The Greenspan type model investigated in [1] is considered to illustrate and test the feasibility of the computational method proposed. This model is appealing for computational testing purposes for two reasons: first, it consists of two decoupled linear elliptic equations with constant coefficients, while the advance of the tumor boundary is governed by an equation involving only two model parameters; second, accurate, two-dimensional numerical simulations using a boundary integral method have been published in [1] and are available for comparison.

The structure of the paper is as follows: Section 2, the mathematical tumor growth model employed in [1] is reviewed; Section 3 provides a brief description of the general formulation of the level set method; Section 4 presents the numerical algorithms in detail; Section 5 contains the numerical experiments performed and a comparison of the results with the boundary integral simulations published in [1]; finally, Section 6 contains some remarks regarding further research.

2. A simple mathematical model of tumor growth

The tumor growth model employed to develop the computational methodology is described in detail in [1], and is only summarized here. Consider a tumor occupying a time-varying domain $D(t)$. The field variable $\sigma = \sigma(\vec{x}, t)$ represents the concentration of nutrient inside the tumor. It is assumed that the tumor is non-necrotic (no region comprised of dead cells) and that there are no inhibitor chemical species. Nutrient is supplied by the blood vessels at a rate $\Gamma(\sigma, \sigma_B)$, where σ_B is the concentration of nutrient in the blood (assumed constant), at a linear rate; the nutrient is absorbed by the living tumor cells at a linear rate as well. Based on the assumption that the time scale necessary for the tumor to undergo significant changes in volume (~days) is typically much larger than the nutrient diffusion time scale (~minutes), the nutrient diffusion inside the tumor is considered quasi-steady. Thus, the continuum mass balance equation for the nutrient inside the domain occupied by the tumor yields the following diffusion equation for $\sigma = \sigma(\vec{x}, t)$:

$$0 = D_N \nabla^2 \sigma - \gamma_B (\sigma - \sigma_B) - \delta_N \sigma \quad in \ D(t) \tag{2.1}$$

where D_N is the diffusion coefficient (constant), the term $-\gamma_B(\sigma - \sigma_B)$ models the blood-tissue nutrient transfer rate (source term), while the last term $\delta_N \sigma$ (δ_N constant) represents the consumption of nutrient by the living tumor cells (sink term). Further, the tumor is modeled as an incompressible fluid with a velocity field $\vec{u} = \vec{u}(\vec{x}, t)$ obeying the continuity equation in $D(t)$:

$$\nabla \bullet \vec{u} = \gamma_T \sigma - \delta_T \quad in \ D(t) \tag{2.2}$$

where the first term in the right hand side expression represents the tumor cell rate of proliferation (mitosis)–assumed a linear function of the nutrient, while the second term represent the tumor cell rate of death (apoptosis). Both γ_T and δ_T in Eq.(2.2) are assumed constant. The velocity field $\vec{u} = \vec{u}(\vec{x}, t)$ is related to the pressure gradient using a relationship similar to Darcy's law:

3

$$\vec{u} = -w_T \nabla p \quad in \;\; D(t) \tag{2.3}$$

where w_T represents the tumor cell mobility (chemotaxis), assumed constant, and $p = p(\vec{x}, t)$ is the fluid pressure inside the domain occupied by the tumor $D(t)$. Combining eqns. (2.2) and (2.3) yields:

$$\nabla^2 p = -\frac{\gamma_T}{w_T}\sigma + \frac{\delta_T}{w_T} \quad in \;\; D(t) \tag{2.4}$$

The coupled linear equations (2.1) and (2.4) represent the governing field equations for the model state variables $\sigma = \sigma(\vec{x}, t)$ (the nutrient concentration inside the tumor) and $p = p(\vec{x}, t)$ (the pressure inside the tumor).

It is assumed that the nutrient concentration at the tumor boundary is the nutrient concentration existent in the tissue outside the tumor–presumed constant and denoted by σ_{out}, i.e.,

$$\sigma\big|_{\partial D(t)} = \sigma_{out} \tag{2.5}$$

The pressure is assumed to satisfy the Young-Laplace relationship on the boundary:

$$p\big|_{\partial D(t)} = \gamma\kappa \tag{2.6}$$

where γ represents the surface tension (here corresponding to cell-cell adhesion forces), while κ is the local curvature. The normal velocity of the tumor boundary, V, is the normal component of the fluid velocity at the boundary:

$$V = \vec{u}\big|_{\partial D(t)} \bullet \vec{n}_{\partial D(t)} = -w_T \nabla p\big|_{\partial D(t)} \bullet \vec{n}_{\partial D(t)} \tag{2.7}$$

where $\vec{n}_{\partial D(t)}$ represents the unit outward normal to the tumor boundary $\partial D(t)$.

Following [1], the model equations and variables are made dimensionless by introducing:

$$L_D = \frac{D_N^{\frac{1}{2}}}{(\gamma_B + \delta_N)^{\frac{1}{2}}} \tag{2.8}$$

$$\lambda_R = \frac{w_T \gamma}{L_D^3}$$

where L_D represents a diffusion-related length scale and λ_R^{-1} represents a relaxation time scale. The following dimensionless variables are defined:

$\bar{\vec{x}} = \dfrac{\vec{x}}{L_D}$ (dimensionless "space")

$\bar{t} = t\lambda_R$ (dimensionless time)

$\bar{\sigma} = \dfrac{\sigma}{\sigma_{out}}$ (dimensionless nutrient concentration)

$\bar{p} = p\dfrac{L_D}{\gamma}$ (dimensionless pressure).

The governing equations (2.1) and (2.4), the boundary conditions (2.5) and (2.6) and the equation of the moving boundary (2.7) become

$$\nabla^2 \bar{\sigma} - \bar{\sigma} + \gamma_B \sigma_B \frac{1}{\sigma_{out}(\gamma_B + \delta_N)} = 0 \quad in \ \overline{\Omega} = \overline{\Omega}(\bar{t}) := D(\vec{\bar{x}}, \bar{t}) \tag{2.9}$$

$$\nabla^2 \bar{p} = -\frac{\gamma_T \sigma_{out}}{\lambda_R} \bar{\sigma} + \frac{\delta_T}{\lambda_R} \quad in \ \overline{\Omega} = \overline{\Omega}(\bar{t}) \tag{2.10}$$

$$\bar{\sigma}\big|_{\partial\overline{\Omega}} = 1 \tag{2.11}$$

$$\bar{p}\big|_{\partial\overline{\Omega}} = \kappa \tag{2.12}$$

$$\bar{V} = -\nabla\bar{p}\big|_{\partial\overline{\Omega}} \bullet \vec{n}_{\partial\overline{\Omega}} \tag{2.13}$$

where in all the above dimensionless equations the derivatives are with respect to the dimensionless variables $\vec{\bar{x}}$ and $\bar{t}$. Further, let

$$\lambda_M = \gamma_T \sigma_{out} \tag{2.14}$$

be the characteristic mitosis rate and define

$$B = \frac{\sigma_B}{\sigma_{out}} \frac{\gamma_B}{\gamma_B + \delta_N} \tag{2.15}$$

(a dimensionless parameter indicating the relative degree of the tumor vascularization). Substituting Eq.(2.14) into Eq.(2.10) yields:

$$\nabla^2 \bar{p} = -\frac{\lambda_M}{\lambda_R} \bar{\sigma} + \frac{\delta_T}{\lambda_R} \quad in \ \overline{\Omega} = \overline{\Omega}(\bar{t}) \tag{2.16}$$

while substituting Eq.(2.15) into Eq.(2.9) yields:

$$\nabla^2 \bar{\sigma} - (\bar{\sigma} - B) = 0 \quad in \ \overline{\Omega} = \overline{\Omega}(\bar{t}) \tag{2.17}$$

Further, if a new dimensionless nutrient "concentration" is defined as:

$$\Gamma = \frac{\bar{\sigma} - B}{1 - B} \tag{2.18}$$

then from Eqns.(2.17) and (2.11) the following boundary value problem is obtained for Γ:

$$\begin{cases} \nabla^2 \Gamma - \Gamma = 0 \quad in \ \Omega = \Omega(t) \\ \Gamma\big|_{\partial\overline{\Omega}} = 1 \end{cases} \tag{2.19}$$

where the "bar" notation in $\overline{\Omega} = \overline{\Omega}(\bar{t})$ has been dropped for simplicity. Finally, the model parameters can be further reduced by introducing the following two dimensionless parameters:

$$G = \frac{\lambda_M}{\lambda_R}(1 - B)$$

$$A = \frac{\dfrac{\delta_T}{\lambda_M} - B}{1 - B} \tag{2.20}$$

Using the above parameter definitions and Eq.(2.18), Eq.(2.16) can be written as follows:

$$\nabla^2(\bar{p} + G\Gamma) = AG \quad in \quad \bar{\Omega} = \bar{\Omega}(\bar{t}) \tag{2.21}$$

If a new dimensionless "pressure" is defined as:

$$P = \bar{p} - (1-\Gamma)G - AG\frac{\bar{\vec{x}} \bullet \bar{\vec{x}}}{2d} \tag{2.22}$$

where d represents the dimension of the domain occupied by the tumor (d=1,2 or 3) , then the following boundary value problem is obtained for P :

$$\begin{cases} \nabla^2 P = 0 \quad in \quad \Omega = \Omega(t) \\ P\big|_{\partial\Omega} = \kappa - AG\frac{(\vec{x} \bullet \vec{x})\big|_{\partial\Omega}}{2d} \end{cases} \tag{2.23}$$

where the "bar" notation in $\bar{\Omega} = \bar{\Omega}(\bar{t})$ and $\bar{\vec{x}}$ has been dropped for simplicity. Lastly, by substituting Eq.(2.22) into Eq.(2.13), the dimensionless normal "velocity" of the tumor boundary becomes (again, dropping the "bar" notation):

$$V = -\nabla P\big|_{\partial\Omega} \bullet \vec{n}_{\partial\Omega} + G\nabla\Gamma\big|_{\partial\Omega} \bullet \vec{n}_{\partial\Omega} - AG\frac{(\vec{n} \bullet \vec{x})\big|_{\partial\Omega}}{d} \tag{2.24}$$

The sets of equations (2.19) and (2.23) represent two decoupled linear elliptic boundary value problems for the unknowns Γ and P respectively; after they have been solved, the new location of the tumor boundary is found using the normal velocity given by Eq.(2.24).

The regimes of tumor growth represented by the model can be characterized in terms of the parameters G and A as follows:

1. **Low vascularization regime**: $G \geq 0, \ A > 0$.

   In the low vascularization regime (including the avascular stage of growth), there are little or no blood vessels reaching inside the tumor to supply nutrient, which for the model here is characterized by $\dfrac{\sigma_B}{\sigma_{out}} \ll 1$

   (i.e., the nutrient supplied by the blood vessels in this regime is considerably lower than the nutrient existing in the tissue outside the tumor volume).
   In this regime Eq.(2.15) yields $B \ll 1$, and subsequently, from the first Eq.(2.20), $G \geq 0$.Also, in this regime, the apoptosis (tumor cell death due to insufficient nutrient levels) rate and the cellular mitosis rate are typically balanced, so it can be assumed that:

   $$\frac{\delta_T}{\lambda_M} \sim 1.$$

   Since $B \ll 1$, it can be further inferred that $B < \dfrac{\delta_T}{\lambda_M}$, and therefore from the second Eq.(2.20) it follows that $A > 0$.

2. **Moderate vascularization regime**: $G \geq 0$, $A \leq 0$.

   In the moderate vascularization regime, more blood vessels have developed that can bring additional amounts of nutrients into the tumor. However, still the dominant role in feeding the tumor is played by the nutrients existent in the tissue:

   $$\frac{\sigma_B}{\sigma_{out}} < 1.$$

   Once again in this regime, $B < 1$, and $G \geq 0$.
   Also, in this regime for the present model, since additional amounts of nutrients are reaching inside the tumor, it can be assumed that the apoptosis rate slows down, while the mitosis rate is promoted, such that

   $$\frac{\delta_T}{\lambda_M} \leq B .$$ This, in turn, leads to $A \geq 0$.

3. **High vascularization regime**: $G < 0, A < 0 \ or \ A > 0$.

   In the high vascularization regime, a dense network of blood vessels is developed and brings considerable amounts of nutrient inside the tumor. This regime is characterized by $\dfrac{\sigma_B}{\sigma_{out}} \gg 1$

   From Eq. (2.15), $B \gg 1$, and subsequently, $G < 0$.

   In this regime, $A < 0$ corresponds to dominant apoptosis ($\dfrac{\delta_T}{\lambda_M} > B$), while

   $A > 0$ (i.e., $\dfrac{\delta_T}{\lambda_M} < B$) can indicate dominant mitosis (promoted by the high levels of nutrients now reaching inside the tumor volume) as well as balanced apoptosis/mitosis.

These three regimes of growth have been clearly identified in [1], based on the evolution of a radially symmetric tumor (both in 2D and in 3D). The authors have found that in the low vascularization regime, the tumor evolution is monotonic and always leads to a stationary radius (depending on the initial tumor radius, either bounded growth or bounded shrinkage may occur), while in the moderate vascularization regime unbounded growth occurs regardless of the tumor initial radius, and finally, in the high vascularization regime unbounded growth may occur depending on the initial radius and the sign of the parameter A (for instance, if the cell apoptosis is dominant in this regime, then the tumor can shrink and disappear).

3. Level set formulation

As previously defined, let $\Omega = \Omega(t)$ denote the domain occupied by the tumor. Let $\Omega^{out} = \Omega^{out}(t)$ denote the region outside the tumor volume, and $\Sigma = \Sigma(t) = \partial\Omega(t)$ (a curve in 2D and a surface in 3D, respectively) be the boundary of the tumor, separating the tumor and the outside tissue. This boundary evolves in time with a normal velocity

V given by Eq. (2.17), and the problem is finding the location of the tumor boundary at later moments in time starting from a known location at the initial moment of time $\Sigma_0 = \Sigma(t=0)$. One way to do so is by employing the level set method introduced by Osher and Sethian in [24] and based in part on the theory and numerics of curve evolution developed by Sethian in [23]. The basic idea behind the level set method is to introduce an additional variable, denoted by

$$\varphi = \varphi(\vec{x},t), \ \vec{x} \in \Omega \cup \Sigma \cup \Omega^{out}, \ t \in [0,\infty],$$

responsible for capturing the front $\Sigma = \Sigma(t)$ in an implicit fashion at each moment in time:

$$\Sigma = \Sigma(t) = \left\{ \vec{x} \mid \varphi(\vec{x},t) = 0 \right\}.$$

The function $\varphi = \varphi(\vec{x},t)$ is the level set function. First, the initial level set function value is set equal to the signed Euclidean distance function to the tumor boundary at the initial moment of time (taken negative inside the tumor and positive outside):

$$\varphi(\vec{x},0) = \begin{cases} -dist(\vec{x},\Sigma_0) \ , \ \vec{x} \in \Omega(t=0) \\ \qquad 0, \quad \vec{x} \in \Sigma_0 \\ dist(\vec{x},\Sigma_0) \ , \ \vec{x} \in \Omega^{out}(t=0) \end{cases} \tag{3.1}$$

At any moment in time, the location of the tumor boundary is given by the zero level set of the level set function. For a particle on the front with the path $\vec{x} = \vec{x}(t)$ one has:

$$\varphi(\vec{x}(t),t) = 0$$

The kinematics governing the motion of the boundary yields:

$$\frac{d\varphi}{dt} = \frac{\partial \varphi}{\partial t} + \nabla \varphi(\vec{x}(t),t) \bullet \frac{d\vec{x}}{dt}(t) = 0 \ , \ \forall t > 0$$

The outward unit normal on the boundary is given in terms of the level set function by:

$$\vec{n} = \frac{\nabla \varphi}{|\nabla \varphi|} \tag{3.2}$$

Substituting (3.2) in the above equation leads to the evolution equation for the level set function (initial value formulation):

$$\frac{\partial \varphi}{\partial t} + F|\nabla \varphi| = 0 \tag{3.3}$$

where $F = F(\vec{x},t), \ \vec{x} \in \Omega \cup \Sigma \cup \Omega^{out}, \ t > 0$ represents what is typically called an "extension velocity" field (i.e., defined everywhere, such that it always matches the given expression of the normal velocity V on the tumor boundary Σ):

$$F(\vec{x},t)\big|_{\vec{x} \in \Sigma(t)} = V(\vec{x},t)\big|_{\vec{x} \in \Sigma(t)} \tag{3.4}$$

Eq. (3.3) correctly moves the boundary with the prescribed normal velocity given by (2.24). In terms of the level set function, the mean curvature is expressed as:

$$\kappa = \nabla \bullet \vec{n} = \nabla \bullet (\frac{\nabla \varphi}{|\nabla \varphi|}) = \frac{\varphi_{xx}\varphi_y^2 - 2\varphi_x\varphi_y\varphi_{xy} + \varphi_{yy}\varphi_x^2}{(\varphi_x^2 + \varphi_y^2)^{\frac{3}{2}}} \tag{3.5}$$

As compared to an explicit front-tracking formulation, there are considerable advantages of the level set formulation:

- the domain occupied by the tumor at each moment of time (where the model equations (2.19), (2.23) must be solved for the unknowns Γ and P respectively) is apparent from the sign of the level set function (here taken negative);
- the geometric properties of the tumor boundary (normal and curvature) are readily available from (3.2) and (3.5) above;
- the same formulation holds regardless of the number of spatial dimensions (1,2 or 3);
- enhanced implementations such as "the narrow band method" introduced by Adalsteinsson and Sethian in [3] or "the fast marching method" (see [2]) are available that make the boundary capturing more computationally efficient.

On the other hand, some challenges arise when implementing the level set method:

- construction of the "extension velocity" field F in the level set equation (3.3) (generally, there is no natural choice for this field which is only defined on the interface itself);
- re-initialization of the level set function φ as a signed distance to the interface $\Sigma(t)$ is needed in two instances: first, steep or flat gradients can develop that will in turn affect the estimation of the geometrical properties of the interface via eqns. (3.2) and (3.5); second, if a "narrow band" type method is used, then the level set function φ must be re-initialized to a signed distance function each time the "narrow band" is rebuilt.

3.1 *Construction of the "extension velocity" field off the interface*

One way of extending the normal velocity off the interface is extrapolation in the normal direction, following characteristics that flow outward from the interface, such that the velocity is constant on rays normal to the interface. This method, introduced by Malladi and Sethian [25], works particularly well when no other information is available except for what is known on the interface–as is the case here. At points adjacent to the interface, on each side, the "extension velocity" field F is first constructed by hand as follows: standing at a grid point adjacent to the interface, either inside the domain occupied by the tumor or outside, find the closest point on the interface whose velocity is given by Eq. (2.24) and copy its velocity. The velocity values at the adjacent points are subsequently kept fixed and framed as boundary conditions for the following linear Hamilton-Jacobi equations (see [5] for the details):

$$\frac{\partial F}{\partial \tau} + \vec{n} \bullet \nabla F = 0 \ \ in \ \Omega^{out}(t) \tag{3.6}$$

$$\frac{\partial F}{\partial \tau} - \vec{n} \bullet \nabla F = 0 \ \ in \ \Omega(t) \tag{3.7}$$

In the above equations (3.6) and (3.7), the local unit outward normal is defined by

$$\vec{n} = \vec{n}(\vec{x}, t) = \frac{\nabla \varphi(\vec{x}, t)}{|\nabla \varphi(\vec{x}, t)|} \tag{3.8}$$

Here τ designates a pseudo-time for the relaxation of the equations to steady-state at each moment of time t. At steady-state, the corresponding solution $F = F(\vec{x}, t)$ will be constant on rays normal to the interface. Construction of the extension velocity field in this manner has the advantage that it tends to preserve the signed distance function during the interface evolution in time.

3.2   *Re-initialization of the level set function φ*

As pointed out above, in general, a procedure is needed to reset the level set function φ as a signed distance function to the interface (in this case, the tumor boundary) from time to time. It is easy to see that the location of the interface $\Sigma = \Sigma(t) = \{\vec{x} \,|\, \varphi(\vec{x}, t) = 0\}$ in time is independent of the particular choice of the initial data $\varphi(\vec{x}, t = 0)$ as long as its zero level set function coincides with the initial (known) location of the interface: $\Sigma_0 = \Sigma(t = 0) = \{\vec{x} \,|\, \varphi(\vec{x}, t = 0) = 0\}$. Thus, re-initialization at some moment of time t can be regarded as the process of replacing the current level set function $\varphi(\vec{x}, t)$ by another function $\varphi^{reinit}(\vec{x}, t)$ that has the same zero contour but is better behaved; $\varphi^{reinit}(\vec{x}, t)$ becomes the new level set function to be used as initial data until the next re-initialization.

As was the case with building the extension velocity field, there is more than one way of re-initializing the level set function φ to a signed distance function to the interface [2, 5, 8]. One approach [5] employs the following "re-initialization equation":

$$\begin{cases} \dfrac{\partial \varphi^{reinit}}{\partial \tau} + S(\varphi_0^{reinit})(|\nabla \varphi^{reinit}| - 1) = 0 \\ \varphi_0^{reinit} = \varphi^{reinit}(\vec{x}, \tau = 0) = \varphi(\vec{x}, t) \end{cases} \tag{3.9}$$

where $S(\varphi_0^{reinit})$ is a sign function taken as +1 in $\Omega^{out}(t)$, -1 in $\Omega(t)$ and 0 on the interface. Here again, τ designates a pseudo-time for relaxing the equation to steady-state at a fixed real time t. By solving Eq. (3.9) to steady-state, the resulting solution $\varphi^{reinit}(\vec{x}, t)$ will be a signed distance function to the interface $\Sigma = \Sigma(t)$ at the particular time t in the model evolution. For better numerical behavior, the "sign" function in Eq.(3.9) is "smeared out" as follows: [5]:

$$S(\varphi_0^{reinit}) = \frac{\varphi_0^{reinit}}{\sqrt{(\varphi_0^{reinit})^2 + h^2}} \tag{3.10}$$

where h represents the size of the fixed Cartesian mesh chosen to discretize the problem. In Eq. (3.9), points near the interface outside the domain occupied by the tumor use the points inside the domain occupied by the tumor as boundary conditions and vice versa. When this circular loop of dependencies eventually balances out, a steady-state solution is reached.

If the initial φ_0^{reinit} is relatively smooth and balanced across the interface, then solving Eq.(3.9) to steady-state works rather well [5]. When a "narrow band" level set method is employed, one is particularly interested in resetting the level set function as accurately as possible to a signed distance function in a narrow region (tube/band) around the interface. This generally happens relatively fast if the initial $\left|\nabla \varphi_0^{reinit}\right|$ does not depart substantially from 1 at points adjacent to the interface on each side, even if a re-initialization has not been performed recently. An alternate choice [5, 8], particularly useful if the initial $\left|\nabla \varphi_0^{reinit}\right|$ is significantly far from 1, is to use:

$$S(\varphi^{reinit}) = \frac{\varphi^{reinit}}{\sqrt{(\varphi^{reinit})^2 + \left|\nabla \varphi^{reinit}\right|^2 h^2}} \tag{3.11}$$

in Eq.(3.9) instead of $S(\varphi_0^{reinit})$.

The advantage of solving equation (3.9) in one pass, rather than solving two separate nonlinear Hamilton-Jacobi equations–one outside the domain occupied by the tumor and one inside, that require preliminary initialization by hand at the grid points adjacent to the interface on each side–is that it readily allows for higher order spatial discretization. The disadvantage is that numerical errors will tend to move the interface to some degree. This can become a problem if re-initialization is performed too often–especially for unstable problems, where it translates into mass/volume loss [2].

4. Description of the numerical algorithm and discretization procedures

The goal here was to develop a general computational framework for use in the numerical investigation of a broader range of tumor growth models. The level set method provides good generality for handling relatively simple or quite complex tumor boundary evolution. Finite differences were chosen to discretize the model equations because of the flexibility that they allow. Another objective was straightforward implementation from an algorithmic point of view. The resulting computational framework can be used for testing and investigating various existing models or new ones that are being developed. The ideas illustrated here for the tumor growth model presented in Section 2 have been successfully applied to obtain numerical simulations in two dimensions using a substantially more complex nonlinear tumor growth model [21].

The following solution formulation is targeted on generality and computational simplicity, but more optimal approaches for the particular problem investigated will be pointed out whenever appropriate. The numerical procedure for the present model solves the pair of Eqs. (2.19) and (2.23), and then updates the location of the tumor boundary using Eq.(2.24). The solution algorithm is outlined in the steps listed below:

1) It is assumed that the level set function $\varphi(\vec{x},t)$ is known at the current time level t and is equal to the signed distance function (prescribed initially, or as a result of re-initialization at later times). As a result, the current location of the interface is implicitly known. A "narrow band" (tube) is built around the interface, with a user-prescribed width (the optimal width for a specific problem depends on the quantities involved, as well as the number of re-initializations employed). Since $\varphi(\vec{x},t)$ is assumed close to a signed

distance function, the narrow band is defined by locating the points using the following criterion:

$$\left\{ \vec{x} \,\middle|\, |\varphi(\vec{x},t)| < width \right\}^{not.} = T .$$

The grid points inside the tube and the grid points near the tube edge are marked distinctly

2) With the location of the boundary implicitly captured by the current level set function $\varphi(\vec{x},t)$, Eqs. (2.19) and (2.23) are solved to obtain the numerical solution for Γ and P at the current time step t.

3) With the values of Γ and P determined at the current time step t, construct the "extension velocity" field $F = F(\vec{x},t)$ as described in Section 3.1, at points $\vec{x}$ inside the narrow band tube T.

4) With the extension velocity field computed at points inside the tube T, the level set equation (3.3) is solved inside the tube to update the level set function at the next time step. The values of the level set function at grid points distinctly marked near the tube edge in Step 1 are frozen, as well as the values of the level set function outside the tube T. The following conditions are monitored:

   a) whether the newly updated tumor boundary (interface) approaches the tube edge to within a specified tolerance (if so, then the values kept frozen in Step 4, which serve as artificial numerical boundary conditions, will severely affect the actual location of the interface);
   b) whether steep or flat gradients are developing in the newly updated level set function, particularly at points neighboring the interface.

Steps 2-4 are repeated until either situation a) or b) occurs; when this happens, the narrow band (tube) T must be rebuilt and the procedure begins with Step 1 again. Employing this Narrow Band Level Set Method is computationally very efficient (especially when constructing the extension velocity field); such an approach is well-suited when only the evolution of the interface itself is of interest (i.e., the zero level set)–as it is the case for the tumor growth problem.

   In what follows, the two-dimensional case is considered. The domain occupied by the tumor Ω is embedded into a larger fixed, time-independent, computational domain $\mathbf{D}$, that is discretized using a uniform Cartesian with $\Delta x = \Delta y = h$. The region outside of the tumor (usually representing healthy tissue) is denoted by $\Omega^{out} = \mathbf{D} \setminus \Omega$. The tumor boundary will often be referred to as the "interface" – separating the domain occupied by the tumor from the outside tissue.

   Fig.1 is a schematic diagram of the tumor boundary located within the narrow band on the Cartesian grid. A "regular" grid point (either inside the domain occupied by the tumor or outside) shall denote a point on the fixed Cartesian grid that has no neighbors on the tumor boundary, in either the horizontal (x) direction or the vertical (y) direction, while an "irregular" grid point (on each side of the tumor boundary) corresponds to a point on the fixed Cartesian grid that is adjacent to the boundary, either horizontally or vertically.

The discrete approximations of the geometric variables (i.e. the normal and the curvature) can be found in Appendix A.

4.1 Discretization of the governing equations

The procedure for solving the boundary value problem (2.23) to determine the dimensionless "pressure" field $P = P(\vec{x}, t)$ is described in detail below. The procedure for the dimensionless nutrient "concentration" $\Gamma = \Gamma(\vec{x}, t)$ is similar and in fact, much simpler, due to the type of boundary condition imposed. Recalling (2.23), the problem to be solved for $P = P(\vec{x}, t)$ is given by:

$$
\begin{cases}
\nabla^2 P = 0 & in \ \Omega = \Omega(t) & (4.1) \\
P\big|_{\partial\Omega} = \kappa - AG \dfrac{(\vec{x} \bullet \vec{x})\big|_{\partial\Omega}}{4} & & (4.2)
\end{cases}
$$

Suppose that the current time is $t_n = n\Delta t$, and the current level set function $\varphi_{i,j}^n = \varphi(x(i), y(j), t_n)$ is known at all Cartesian grid points (i, j). Then the current domain occupied by the tumor is $\Omega_n = \Omega(t_n)$. Eq.(4.1) with the boundary condition (4.2) must be solved at points $(i, j) \in \Omega_n$ to obtain the discrete solution $P_{i,j}^n = P(x(i), y(j), t_n)$ at the current time step. The grid points (i, j) marked as "irregular" on each side of the tumor boundary in Fig.1 are determined by checking to see if the level set function changes sign either in the horizontal direction, or in the vertical direction, or in both; if so, that means the interface cuts through the grid cell containing the current grid point, and that makes it an "irregular" grid point. Other grid point are marked as "regular". At "regular" grid points $(i, j) \in \Omega_n$, the standard 5-points stencil is used to discretize the Laplace operator in (4.7):

$$
\frac{P_{i+1,j}^n - 2P_{i,j}^n + P_{i-1,j}^n}{h^2} + \frac{P_{i,j+1}^n - 2P_{i,j}^n + P_{i,j-1}^n}{h^2} = 0 \tag{4.3}
$$

Consider now the case of an "irregular" horizontal grid point $(i, j) \in \Omega_n$, where, for instance, $\varphi_{i,j}^n < 0$ and $\varphi_{i+1,j}^n > 0$. Then there is an interface point in the horizontal direction, in between $x(i)$ and $x(i+1)$, call it x_b. By linear interpolation of the level set function, the value of x_b can be determined as follows:

$$
x_b - x(i) = -\left(\frac{\varphi_{i,j}^n}{\varphi_{i+1,j}^n - \varphi_{i,j}^n}\right)h \overset{not.}{=} \theta_x h \qquad (0 < \theta_x < 1) \tag{4.4}
$$

Next, a second-order interpolating polynomial $p(x)$ in the x-direction is formally constructed using $h, \theta_x, P(x_b, y(j), t_n), P_{i,j}^n, P_{i-1,j}^n$ respectively. Note that $P(x_b, y(j), t_n)$ is computed from the boundary condition (4.2) applied at the boundary point $(x_b, y(j))$,

13

where the curvature is estimated as described in Appendix A and x_b is known from (4.4). Thus, with the expressions of the interpolated polynomial formally computed, the second derivative is approximated as follows:

$$\frac{\partial^2 P^n_{i,j}}{\partial x^2} \approx p''(x)\big|_{x=x(i)} \tag{4.5}$$

A similar procedure is used in the y-direction. Of course, there will be "irregular" grid points that might have neighbors on the boundary both in the x- and y-direction.

Finally, considering both "regular" grid points as well as "irregular" ones inside the domain occupied by the tumor at the current moment of time, the system of discrete equations that must be solved to determine the unknowns $\{P^n_{i,j}\}\big|_{(i,j)\in\Omega_n}$ can be cast in the general form:

$$P^n_{i,j} = f_{i,j}(P^n_{i-1,j}, P^n_{i+1,j}, P^n_{i,j-1}, P^n_{i,j+1}),\ (i,j)\in\Omega_n \tag{4.6}$$

where

$$f_{i,j}(P^n_{i-1,j}, P^n_{i+1,j}, P^n_{i,j-1}, P^n_{i,j+1}) = a_{i,j} + b_{i,j}\, P^n_{i-1,j} + c_{i,j}\, P^n_{i+1,j} + d_{i,j}\, P^n_{i,j-1} + e_{i,j}\, P^n_{i,j+1} \tag{4.7}$$

A straightforward and general way of solving the system (4.13) for average mesh sizes is by the iterative Gauss-Seidel method. The use of a Gauss-Seidel method here has the advantage of generality and it only requires very modest memory storage. Numerical tests were performed to examine the optimal stopping criterion in the 2-norm,

$$\left(\sum_{(i,j)\in\Omega_n}\left|P^{n,M+1}_{i,j} - P^{n,M}_{i,j}\right|^2\right)^{\frac{1}{2}} < tol\ .$$

For the present calculations, for values $10^{-6} \le tol \le 10^{-12}$, no differences were observed in the converged solution of (4.6); therefore, the value $tol = 10^{-6}$ was used for all the solutions.

4.2   Numerical construction of the "extension velocity" field

As described in Section 3.1, the extension velocity field $F = F(\vec{x},t)$ at a particular moment of time t (when the level set function $\varphi = \varphi(\vec{x},t)$ and the model field variables $P = P(\vec{x},t)$, $\Gamma = \Gamma(\vec{x},t)$ are known) is obtained by solving Eqs. (3.6) and (3.7) to steady-state. First, at grid points adjacent to the interface on each side marked as "irregular" in Fig.1, the extension velocity field is constructed by hand. Two ways of doing this are described in Appendix B. A numerical estimate of the normal velocity is needed at points on the interface $\vec{x}_{interface}$ – whose expression is given by Eq. (2.24):

$$V(\vec{x}_{interface},t) = -(\nabla P \bullet \vec{n})\big|_{(\vec{x}_{interface},t)} + G(\nabla\Gamma \bullet \vec{n})\big|_{(\vec{x}_{interface},t)} - AG\frac{(\vec{n}\bullet\vec{x})\big|_{(\vec{x}_{interface},t)}}{2} \tag{4.8}$$

The local unit outward normal to the interface $\vec{n} = \vec{n}(\vec{x}_{interface},t)$ in (4.8) is computed as described in Appendix A. Then, the normal derivatives in (4.8), both for P and Γ, are approximated by using backward differencing in the normal direction; here, a second-

order backward difference formula is employed (more explanations on this particular choice in section 5. ahead):

$$(\nabla P \bullet \vec{n})\Big|_{(\vec{x}_{\text{int erface}}, t)} \approx \frac{3P(\vec{x}_{\text{int erface}}, t) - 4P(\vec{x}_{\text{int erface}} - h\vec{n}, t) + P(\vec{x}_{\text{int erface}} - 2h\vec{n}, t)}{2h}$$
(4.9)

where, according to the boundary condition (2.23) on P,

$$P(\vec{x}_{\text{int erface}}, t) = \kappa(\vec{x}_{\text{int erface}}, t) - AG\frac{((\vec{x}_{\text{int erface}}) \bullet (\vec{x}_{\text{int erface}}))}{4}$$
(4.10)

and the curvature $\kappa(\vec{x}_{\text{int erface}}, t)$ is computed as described in Appendix A.

The terms $P(\vec{x}_{\text{int erface}} - h\vec{n}, t)$ and $P(\vec{x}_{\text{int erface}} - 2h\vec{n}, t)$ in (4.9) above are estimated using bilinear interpolation from the known values of P at the 4 neighboring corners on the fixed Cartesian grid at the current moment of time t. Similarly for Γ, where the value $\Gamma(\vec{x}_{\text{int erface}}, t) = 1$, according to the boundary condition in (2.19). Finally, eqns. (3.6) and (3.7) respectively must be solved to steady-state, within the current tube T, by using the previously estimated values of the extension velocity at irregular grid points as boundary conditions. Everywhere else inside the current tube the extension velocity field is initialized to 0.

Equations (3.6) and (3.7) are each a linear hyperbolic equation of the form:

$$\frac{\partial F}{\partial \tau} + a(x, y)\frac{\partial F}{\partial x} + b(x, y)\frac{\partial F}{\partial y} = 0$$
(4.11)

with $a(x, y)$ and $b(x, y)$ given. Here τ represents a pseudo-time that is distinct from the real time t (which is fixed for Eq.(4.26)). A regular first order up-wind differencing scheme [13, 14] is used to discretize Eq.(4.26) :

$$F_{i,j}^{k+1} = F_{i,j}^{k} - \Delta\tau[\max(a_{i,j}, 0)D^{-x}F_{i,j}^{k} + \min(a_{i,j}, 0)D^{+x}F_{i,j}^{k} +$$
$$+ \max(b_{i,j}, 0)D^{-y}F_{i,j}^{k} + \min(b_{i,j}, 0)D^{+y}F_{i,j}^{k}]$$
(4.12)

where:

$$D^{-x}F_{i,j}^{k} = \frac{F_{i,j}^{k} - F_{i-1,j}^{k}}{h}, \ D^{+x}F_{i,j}^{k} = \frac{F_{i+1,j}^{k} - F_{i,j}^{k}}{h}$$

$$D^{-y}F_{i,j}^{k} = \frac{F_{i,j}^{k} - F_{i,j-1}^{k}}{h}, \ D^{+y}F_{i,j}^{k} = \frac{F_{i,j+1}^{k} - F_{i,j}^{k}}{h}$$

The time-step $\Delta\tau$ must obey the CFL stability condition:

$$\Delta\tau \max_{i,j}\{\frac{|a_{i,j}|}{h} + \frac{|b_{i,j}|}{h}\} \leq 1$$
(4.13)

Since in this case, $|a_{i,j}| \leq 1$ and $|b_{i,j}| \leq 1$, choosing a time step $\Delta\tau \leq \frac{h}{2}$ will automatically satisfy (4.13).

In the numerical experiments presented in section 5., $\Delta\tau = \dfrac{h}{5}$ and equation (4.12) is iterated until $\max\limits_{i,j}\left|F_{i,j}^{k+1} - F_{i,j}^{k}\right| < h^2\Delta\tau$ (consistent with the order of the spatial approximation). The resulting solution $\{F_{i,j}\} = \{F_{i,j}(t)\}$ is the extension velocity at the current real time t.

4.3 Discretization of the level set equation and the re-initialization equation

The level set equation (3.3) is discretized using a conservative scheme for nonlinear Hamilton-Jacobi equations with convex Hamiltonian [2]:

$$\varphi_{i,j}^{n+1} = \varphi_{i,j}^{n} - \Delta t[\max(F_{i,j}^{n},0)\nabla^{+} + \min(F_{i,j}^{n},0)\nabla^{-}] \tag{4.14}$$

where:

$$\varphi_{i,j}^{n} = \varphi(x(i), y(j), n\Delta t)$$

$$F_{i,j}^{n} = F(x(i), y(j), n\Delta t)$$

$$\nabla^{+} = [\max(D^{-x}\varphi_{i,j}^{n},0)^2 + \min(D^{+x}\varphi_{i,j}^{n},0)^2 + \max(D^{-y}\varphi_{i,j}^{n},0)^2 + \min(D^{+y}\varphi_{i,j}^{n},0)^2]^{\frac{1}{2}} \tag{4.15}$$

$$\nabla^{-} = [\max(D^{+x}\varphi_{i,j}^{n},0)^2 + \min(D^{-x}\varphi_{i,j}^{n},0)^2 + \max(D^{+y}\varphi_{i,j}^{n},0)^2 + \min(D^{-y}\varphi_{i,j}^{n},0)^2]^{\frac{1}{2}} \tag{4.16}$$

and D^{-x} (D^{-y}) stands for the backward differencing approximation of the first-order partial derivative in the x (y)–direction, while D^{+x} (D^{+y}) stands for the forward differencing approximation. The above scheme is a first order (forward Euler) in time.
The backward and forward difference approximations in (4.15) and (4.16) can be computed by employing first-order spatial discretization, or via higher-order schemes, such as HJ ENO or WENO [5]. The time step in (4.14) must obey the CFL condition for stability:

$$\Delta t \max\limits_{i,j} F_{i,j}^{n} \le \dfrac{h}{2} \tag{4.17}$$

In practical applications, the level set motion generally tends to show much less sensitivity to temporal accuracy (once the time step is carefully chosen to insure convergence), while the spatial accuracy seems to be far more important. Although, typically, higher order spatial schemes (like fifth order HJ WENO) are coupled with higher order schemes in time (like third order TVD RK, [5]), a first order forward Euler in time can often be safely employed, thus significantly reducing the computational cost. For the problem investigated here, numerical experiments have shown no visible sensitivity to reductions in the time-step by a factor of 10 or even 100 in a forward Euler method, once the time step is carefully chosen such that convergence occurs. The numerical simulations show notable sensitivity to spatial accuracy in the low vascularization regime, where the tumor evolution predicted by the model here investigated proves bounded but unstable; in the high vascularization regime (stable evolution) a first order spatial discretization and a fifth order WENO spatial discretization yield results almost indistinguishable at plotting.

The discrete level set Eq.(4.14) is only being solved within the current narrow band tube T; the values of the level set function at the grid points marked "near a tube edge" are kept frozen, as well as the grid points outside the current tube. More details on the narrow band implementation are given in Section 5.

The re-initialization Eq. (3.9)–either with the choice (3.10) or (3.11)–is discretized using the same conservative scheme for Hamilton-Jacobi equations as in (4.30) above [8]:

$$\varphi_{i,j}^{reinit,k+1} = \varphi_{i,j}^{reinit,k} - \Delta\tau[\max(S_{i,j}^k,0)(\nabla^+ - 1) + \min(S_{i,j}^k,0)(\nabla^- - 1)] \qquad (4.18)$$

where:

$$\varphi_{i,j}^{reinit,k} = \varphi^{reinit}(x(i), y(j), k\Delta\tau)$$

$$S_{i,j}^k = S(\varphi^{reinit}(x(i), y(j), k\Delta\tau))$$

$$\nabla^+ = [\max(D^{-x}\varphi_{i,j}^{reinit,k},0)^2 + \min(D^{+x}\varphi_{i,j}^{reinit,k},0)^2 + \max(D^{-y}\varphi_{i,j}^{reinit,k},0)^2 + \min(D^{+y}\varphi_{i,j}^{reinit,k},0)^2]^{\frac{1}{2}}$$

$$\nabla^- = [\max(D^{+x}\varphi_{i,j}^{reinit,k},0)^2 + \min(D^{-x}\varphi_{i,j}^{reinit,k},0)^2 + \max(D^{+y}\varphi_{i,j}^{reinit,k},0)^2 + \min(D^{-y}\varphi_{i,j}^{reinit,k},0)^2]^{\frac{1}{2}}$$

Whenever re-initialization is required, Eq. (4.18) is iterated to steady-state. If (3.10) is used for the smeared "sign" function S, then S is evaluated only once in (4.18), using the initial data $\varphi_{i,j}^{reinit,0} = \varphi^{reinit}(x(i), y(j),0)$; on the other hand, if (3.11) is being used, then $S = S(\varphi^{reinit})$ must be updated continually at each iteration in (4.18). Both choices have been numerically tested for the current problem; no visible differences have been observed. The same comments made in Section 4.3 hold regarding the order of the temporal and spatial approximations in (4.18). If forward Euler in time and fifth-order discretization in space are used in the level set equation (4.14), then they are used in the re-initialization equation (4.18) for consistency.

Remark:

Particularly for the unstable regime of the tumor growth, frequent use of re-initialization is avoided unless required. Re-initialization is used here jointly with the reconstruction of the "narrow band" (tube), and then, according to Step 1 in the algorithm, the level set function is reset to a signed distance function in the entire computational domain in order to correctly mark the grid points inside the new tube. Otherwise, if intermediate re-initializations are desired without re-building the tube, the discrete re-initialization equation (4.34) can be iterated to steady-state inside the current tube T only.

5. Numerical results

In order to test the solution procedures, a series of two-dimensional numerical simulations of tumor growth governed by the model introduced in Section 2 are presented, along with additional details of the solution implementation. The results are compared quantitatively to the linear theory and qualitatively to the boundary integral solutions presented in [1]. For the model governed by equations (2.19), (2.23) and (2.24)

(namely, decoupled linear elliptic equations with constant coefficients), the boundary integral method is an optimal choice from the point-of-view of accuracy and efficiency. The objective of the present work is to provide a general computational framework that may be used successfully for more complex tumor growth models (e.g., coupled parabolic equations, variable coefficients, different governing equations inside and outside the tumor domain, etc. [21]), for which a boundary integral method is no longer applicable. Additionally, the proposed methodology can be extended to three-dimensional simulations in arbitrary geometries.

For the level set computations, the first issue to be addressed is the choice of the "narrow band" (tube) width. While in [2], a width $6h \leq width \leq 9h$ on each side of the interface has been suggested as generally optimal, the appropriate width for a specific problem must be chosen depending on the quantities involved in the interface evolution in time (e.g., curvature), the order of the spatial discretization in the level set equation (4.14) and the number of re-initializations allowed. Since in the narrow band approach the level set function is updated only within the tube, its values at grid points near the edges of the tube boundary are frozen (as well as values outside the tube that are not used until the tube is rebuilt). The interface (identified as the zero level set) cannot be allowed to move all the way to the tube boundary, since the artificial boundary conditions there would adversely affect the motion of the zero level set as well as its geometric properties (i.e., normal, curvature). In [3], it has been suggested that for flows under curvature, a better approach is to estimate the derivatives in (4.14) at points near the edge of the tube boundary by linear extrapolation from within the tube, instead of freezing the values of the level set function. However, rather than employing this more sophisticated approach for the current implementation, the interface is always maintained at a safe distance from the boundary of the tube, even if this translates into a wider tube and more frequent reconstruction of the tube. If a fifth-order HJ WENO scheme is used to approximate the backward/forward difference operators in (4.15) and (4.16) (requiring 3 neighboring grid points in each up-wind direction), the width of the tube is taken to be $15h$ on each side of the interface. The interface is only allowed within at most 9 grid cells from the tube boundary (i.e., it is allowed to move at most 6 grid cells within the tube) before the tube is rebuilt. If a regular first-order scheme is used in (4.15) and (4.16), then the width of the tube is taken to be $9h$ on each side of the interface and the interface is as before, allowed to move at most 6 grid cells within the tube before the tube rebuilding procedure is triggered.

All the results included here were obtained using the explicit Euler method in time for the level set equation (4.14). Even though the method is first-order in time and fifth-order in space, the truncation error in time and space remain reasonably balanced because of the stability restrictions on the size of the time step. In all the results included here, the mesh size will be indicated rather than the number of points on the fixed Cartesian grid. This is because for the same tube width, a slightly different size for the computational domain might be used for different mesh sizes (i.e., a slightly wider tube for larger mesh sizes, in order for the tube to remain safely embedded in the larger fixed Cartesian grid by the end of the simulation). Additionally, in the figures some of the computational domains have been rescaled for plotting purposes.

18

First, in Fig. 2, the validity of the "narrow band" approach is tested by direct comparison with the corresponding results obtained using a full matrix approach. The initial tumor boundary is a perturbed circle defined by the parametric equation:

$$(x(\alpha), y(\alpha)) = (2.1 + 0.5\cos(2\alpha))(\cos(\alpha), \sin(\alpha)), \alpha \in [0, 2\pi] \qquad (5.1)$$

The values of the dimensionless model parameters are $G = 20, A = 0.5$. According to the model assumptions in Section 2, the tumor is in the low vascularization regime. The mesh size and time step used are listed in the figure caption. Both approaches yield the same tumor evolution to within the truncation error. For both the "narrow band" and the full matrix approach, the fifth-order HJ WENO spatial discretization was used in the level set equation; moreover, the re-initialization procedure (only used in the "narrow band" approach) employs a similar fifth-order HJ WENO spatial discretization for Eq. (4.18). As described in Section 4, for the "narrow band" approach, the re-initialization procedure is always used jointly with the tube reconstruction.

In developing the solution procedure, it was important to understand the impact of the spatial scheme used for the level set solution. In Fig. 3, for the same initial tumor boundary, model parameters and mesh size as the previous case, the tumor boundary evolution at a specific time is shown for two solution methods. The initial tumor shape is shown as the lighter solid oval curve. At a scaled time of 2.5, the dashed curve corresponds to the tumor boundary computed using a first-order scheme for the level set equation (4.14) and the solid curve corresponds to the fifth-order HJ WENO. The narrow band approach was used in both cases. The first-order scheme was not able to properly capture the boundary evolution in the region where the curvature changed most rapidly. Unless otherwise specified the remaining results presented were calculated using the fifth-order HJ WENO scheme both for the level set and for the reinitialization equations.

A simple quantitative check on the solution procedure is provided by a comparison with the growth of angular perturbations to a radially symmetric tumor boundary. The linear stability theory presented in [1] was employed in Mathematica to compute the predicted tumor boundary shape at early times. For the same initial perturbation shape and parameters used in Figs. 2 and 3, Fig. 4 shows the tumor boundary predicted by the linear analysis and the nonlinear solution calculated using the level set approach at three time levels. At each time level, the initial perturbed circular shape is shown as well. At the two earlier times shown, the nonlinear solution tracks the evolution predicted by the linear theory very well. Only at the latest time level shown, where the boundary has grown beyond the validity of the linear theory, does the nonlinear tumor boundary shape differ significantly from the predicted linear shape.

Fig. 5 shows in detail the time evolution of the tumor from the level set solution, again for the same parameters, but calculated using a finer mesh: $h = 0.09$. The same qualitative behavior in the tumor boundary evolution is obtained as displayed by the boundary integral solution presented in figure 2 of [1] for the model parameters G = 20, A = 0.5. Here, a larger symmetric initial perturbation was used because, for the particular case of a very slightly perturbed circle with this choice of the model parameters, replicating the high resolution provided by the boundary integral technique proved difficult due to mesh size limitations. As shown in Fig. 4, at early times the tumor grows in a bounded but unstable fashion with the linear and nonlinear solution overlapping but

19

gradually start to deviate. The linear solution tends to pinch-off, which eventually yields two separate lobes, while the nonlinear evolution of the tumor boundary in time tends to be stabilized by the surface tension (here modeling cell-cell adhesive forces) that oppose the development of large negative curvatures leading to pinch-off. Instead, the tumor continues to grow into a "dogbone" shape with elongated lobes that eventually connect. From the standpoint of model predictions, this type of behavior would lead to engulfing healthy tissue.

In Fig. 6, the time evolution of an asymmetric, multimodal initial tumor is investigated for $G = 20, A = 0.5$. Again, the results were obtained by using a "narrow band" approach, with a fifth-order HJ WENO spatial scheme both in the level set equation (4.14) and the re-initialization equation (4.18); the mesh size is $h = 0.09$. The initial asymmetric tumor boundary is given by:

$$(x(\alpha), y(\alpha)) = (2 + 0.24\cos(2\alpha) + 0.2\sin(2\alpha) + 0.12\cos(3\alpha) +$$

$$+ 0.1\sin(3\alpha) + 0.08\cos(5\alpha) + 0.14\sin(6\alpha))(\cos(\alpha), \sin(\alpha)), \qquad (5.2)$$

$$\alpha \in [0, 2\pi]$$

The results show good qualitative agreement with the corresponding results obtained in [1] using a boundary integral method and the identical asymmetric, initial perturbation. Similarly to the results in [1], Fig. 6 shows modes 2 to 6 becoming unstable as the tumor continues to grow in time, exhibiting the same tendency to form lobes – asymmetric in this case – that will again tend to connect and encapsulate healthy tissue.

Up to this point, all of the cases used to test the level set solution procedure have been in the low vascularization regime of the model. Figure 7 shows two sets of results obtained in the high vascularization regime, for a choice of the model parameters $G = -5, A = 0.2$, and the initial tumor boundary defined by

$$(x(\alpha), y(\alpha)) = (2 + 0.24\cos(2\alpha) + 0.2\sin(2\alpha) + 0.12\cos(3\alpha) +$$

$$+ 0.1\sin(3\alpha))(\cos(\alpha), \sin(\alpha)), \qquad (5.3)$$

$$\alpha \in [0, 2\pi]$$

A "narrow band" approach was used with the two different spatial schemes again evaluated for obtaining the tumor boundary evolution. The results shown in the top part of the figure were obtained using a first-order scheme for both the level set equation and for the re-initialization equation; on the bottom part of the figure a fifth-order HJ WENO scheme was used for both equations. In both cases, the mesh size is $h = 0.05$. In this case, there are no notable differences between the two sets of results (unlike the unstable growth case in the low vascularization regime depicted in Figs. 2 and 3). It is important to note that similar comparisons using courser meshes ($h = 0.1$ and $h = 0.2$) for this case showed no notable differences between results obtained via the two different spatial discretization methods. Also, comparisons against the full matrix approach at a mesh size of $h = 0.1$ were in agreement with the "narrow band" approach. The choice of the model parameters, $G = -5, A = 0.2$, here corresponds to a scenario where cell apoptosis rate is higher than cell mitosis rate – which in this model leads to tumor shrinkage and eventual disappearance. As it can be seen in Fig. 7, the shrinkage occurs in a stable fashion (in this regime, the initially perturbed tumor boundary quickly evolves into a shrinking circle).

Finally, the results presented in Fig. 8 show the tumor evolution in time in the high vascularization regime as well, corresponding to a scenario where the mitosis rate is

higher than apoptosis rate. The simulation starts from the same initial tumor shape used for the previous case, Eq. (5.3). In Fig. 8, the model parameters, $G = -5, A = 0.8$, were used. In this case stable, unbounded growth occurs (in this regime, the initially perturbed tumor very soon evolves into an expanding circle). The results shown in both Figs. 7 and 8 show very good agreement with results presented in [1] obtained via the boundary integral method.

Additional quantitative information regarding the solution procedure was obtained from a systematic evaluation of the order of spatial accuracy of the overall solution procedure. A mesh refinement analysis was conducted for two cases: one–in the low vascularization regime with model parameters $G = 20, A = 0.5$ and initial tumor boundary given by Eq. (5.2); two–in the high vascularization regime with $G = -5, A = 0.2$ and the initial tumor boundary given by Eq. (5.3). In both cases, the results were obtained using the narrow band approach with the fifth-order HJ WENO in the level set equation and in the re-initialization equation.

As described in Section 4.2, in computing the normal velocity of the tumor interface via Eq. (4.8), a second-order backward difference approximation (4.9) in the normal direction is employed. In theory, since the field variables P and Γ are determined with second-order accuracy, then the numerical value of the normal velocity of the interface can only be first-order accurate in this approach – regardless of the order of the backward differencing scheme used to approximate the normal derivatives in (4.23). In practice, numerical tests have shown that using first-order backward differencing to approximate the terms $(\nabla P \bullet \vec{n})\big|_{(\vec{x}_{\mathrm{int}\,erface},t)}$ and $(\nabla \Gamma \bullet \vec{n})\big|_{(\vec{x}_{\mathrm{int}\,erface},t)}$ in (4.8) leads to considerably slower motion than when a second-order approximation is used. Further comparison of the tumor evolution in time using a second-order approximation and a third-order approximation showed no visible difference. Therefore, the second-order approximation (4.9) was chosen for the implementation here. A second related aspect must be noted here as well: according to the observations in the precedent paragraph, the numerical treatment of the term $(\nabla \Gamma \bullet \vec{n})\big|_{(\vec{x}_{\mathrm{int}\,erface},t)}$ is first-order accurate; thus, the magnitude of the model parameter G that multiplies this term in (4.8) is expected to have an important impact on the tumor evolution in time. This will be clearly shown in the mesh refinement analysis below.

Fig. 9 shows the evolution of the tumor boundary at three different moments of time computed using three different mesh sizes: $h = 0.36$, $h = 0.18$ and $h = 0.09$ for $G = 20$, $A = 0.5$ and the initial tumor boundary given by Eq. (5.2). Figure 10 shows the evolution of the tumor at three different moments of time computed using three different mesh sizes: $h = 0.4$, $h = 0.2$ and $h = 0.1$ for $G = -5$, $A = 0.2$ and the initial tumor boundary given by Eq. (5.3). By comparison, it is very clear that for the case with the larger magnitude of G, the tumor evolution in time is much more sensitive to the mesh size than the smaller G case. The mesh sizes were chosen to allow for two levels of refinement, starting with a relatively coarse mesh. Since, ideally, the methodology developed here is designed for implementation on moderately sized, standalone computing platforms, coarser meshes were used to evaluate the solution behavior and determine whether the results show the correct qualitative trends.

The final issue addressed is the overall accuracy of the method here employed. Once the boundary starts to move, it becomes difficult to perform a quantitative convergence analysis on the field variables $\{P_{i,j}^n\}_{i,j\in\Omega_n}$ and $\{\Gamma_{i,j}^n\}_{i,j\in\Omega_n}$ in the vicinity of the moving boundary at a particular moment of time $t = t_n$, since grid points might lie on different sides of the boundary for different mesh sizes. Instead, the accuracy of the tumor boundary location in time can be quantitatively estimated. The level set method reconstructs the interface at every moment of time as a piecewise linear manifold; suppose that the Cartesian mesh size is doubled twice and denote by $\{\vec{x}_{\text{interface},k}^{n,1}\}\big|_{k=\overline{1,N_1}}$,

$\{\vec{x}_{\text{interface},k}^{n,2}\}\big|_{k=\overline{1,N_2}}$ and $\{\vec{x}_{\text{interface},k}^{n,4}\}\big|_{k=\overline{1,N_4}}$ the collection of interface points

$\vec{x}_{\text{interface},k}^{n} = (x_{\text{interface},k}, y_{\text{interface},k})$ at time $t = t_n$ corresponding to the coarsest mesh, the intermediate mesh and the finest mesh, respectively (it is assumed that the interface here is a closed curve). Thus, the interface is represented as a closed polygonal line with N_1, N_2 and N_4 line segments for the coarsest, intermediate and finest representation, respectively. Let the lengths of these polygonal lines be denoted by L_1, L_2 and L_4 respectively. The idea is to re-divide each polygonal line into the same given number N of equally spaced points (typically $N = N_4$). Start from the same position for all three polygonal lines – say the point on each polygonal line that lies on the x-axis closest to 0 – and move clockwise along each polygonal line with a step $s_1 = \dfrac{L_1}{N}$, $s_2 = \dfrac{L_2}{N}$ and

$s_4 = \dfrac{L_4}{N}$; mark the newly determined points on each polygonal line L_1, L_2 and L_4, yielding $\{\vec{X}_{\text{interface},k}^{n,1}\}\big|_{k=\overline{1,N}}$, $\{\vec{X}_{\text{interface},k}^{n,2}\}\big|_{k=\overline{1,N}}$ and $\{\vec{X}_{\text{interface},k}^{n,4}\}\big|_{k=\overline{1,N}}$.

Since no analytic solution is available, the errors are computed with respect to the numerical solution corresponding to the finest mesh $\{\vec{X}_{\text{interface},k}^{n,4}\}\big|_{k=\overline{1,N}}$; following [9],[11], the error at time $t = t_n$ is defined as the largest Euclidean distance of the corresponding points of the two computed interfaces:

$$e_{4\_1}^n = \max_{k=1,N}\left|\vec{X}_{\text{interface},k}^{n,1} - \vec{X}_{\text{interface},k}^{n,4}\right| \tag{5.4}$$

$$e_{4\_2}^n = \max_{k=1,N}\left|\vec{X}_{\text{interface},k}^{n,2} - \vec{X}_{\text{interface},k}^{n,4}\right| \tag{5.5}$$

A ratio $e_{4\_1}^n / e_{4\_2}^n$ between 4 and 5 typically indicates second-order spatial accuracy, while a ratio between 2 and 3 typically indicates first-order spatial accuracy [9, 11].
The quantitative errors resulting from the mesh refinement analysis in Fig. 9 and Fig. 10 are recorded in Table 1 and Table 2, respectively. According to these values, the tumor boundary location using the fixed Cartesian mesh, "narrow band" level set approach developed here is indeed found with first-order spatial accuracy along its evolution in

time. Moreover, the absolute errors are confirmed much larger for the case $G = 20$ than for the case with $G = -5$.

6. Conclusions

A well-established, continuum-based tumor growth model was used here for testing the implementation of the level set approach for simulating tumor evolution. The model was chosen because of the availability of published results for comparison. A rather detailed description of the level set implementation is provided for the purpose of enabling the use of the methodology for a variety of tumor growth models. In the present model, there are no anisotropies included and the interaction of the tumor with its surroundings is incorporated only in simplistic manner.

As is well-established [17], tumor vascularization occurs through tumor induced angiogenesis–a process during which the tumor living cells release a chemical TAF (tumor angiogenic factor). The TAF diffuses into the healthy surrounding tissue and stimulates the capillary network existent nearby outside the tumor–thus leading to formation of new blood vessels through accumulation of newly born endothelial cells; the new capillaries move towards the source of angiogenic factor leading to tumor vascularization. These crucial mechanisms associated with the angiogenesis phenomena are not accounted for in this simplified model.

One of the advantages of the computational framework described here and illustrated in the context of a simplified tumor growth model is its potential applicability to a host of tumor growth models [18, 19]; recently it has been used successfully to generate numerical simulations for a complex model derived from the theory of mixtures and centered on the angiogenesis phenomena [21].

Another advantage comes from the fact that the same exact computational framework is readily adaptable to three dimensional calculations from an algorithmic point of view. All the numerical schemes involved extend to the three dimensional case in a straightforward manner–often translating to simply adding one more dimension to the arrays involved. Moreover, the level set method in the narrow band implementation has the ability of naturally capturing potential large topological changes in the tumor boundary evolution in time at reduced computational expense, while automatically providing information about the local geometric properties. As already mentioned, this proves to be very important in complex tumor growth models where different biological phenomena may occur inside the tumor and outside in the healthy surrounding tissue.

References:

[1] V. Cristini, J. Lowengrub and Q. Nie, *Nonlinear Simulation of Tumor Growth*, J. Math. Biol. **46,** 191-224 (2003)

[2] J.A. Sethian, *Level Set Methods and Fast Marching Methods*, Cambridge University Press, (1999)

[3] D. Adalsteinsson, J.A. Sethian, *A Fast Level Set Method for Propagating Interfaces,* J. Comp. Phys. **118, 2,** 269-277 (1995)

[4] D. Adalsteinsson, J.A. Sethian, *The fast construction of extension velocities in level set methods*, J. Comp. Phys. **148**, 2-22 (1999)

[5] S. Osher and R. Fedkiw, *Level Set Methods and Dynamic Implicit Surfaces,* Springer-Verlag, New York (2002)

[6] S. Chen, B. Merriman, S.Osher and P.Smereka, *A Simple Level Set Method for Solving Stefan Problems,* J.Comp. Phys. **135**, 8-29 (1997)

[7] F. Gibou, R. Fedkiw, R. Caflisch and S. Osher, *A Level Set Approach for the Numerical Simulation of Dendritic Growth,* J. Sci. Comput. **19**, 183-199 (2003)

[8] D. Peng, B. Merriman, S. Osher, H. Zhao and M. Kang, *A PDE-Based Fast Local Level Set Method,* J. Comp. Phys. **155,** 410-438 (1999)

[9] T.Y. Hou, Z. Li, S. Osher and H. Zhao, *A Hybrid Method for Moving Interface Problems with Application to Hele-Shaw flow,* J. Comp. Phys. **134** (1997)

[10] M. Sussman and E. Fatemi, *An Efficient, Interface Preserving Level Set Re-Distancing Algorithm and its Applications to Interfacial Incompressible Fluid Flow,* SCI COMPUT **20**, 1165-1191 (1999)

[11] R.L. LeVeque and Z. Li, *Immersed Interface Methods for Stokes Flow with Elastic Boundaries or Surface Tension,* SIAM J. Sci. Comput. **18, 3,** 709-735 (1997)

[12] Y. Kim, N. Goldenfeld and J. Dantzig, *Computation of Dendritic Microstructures using a Level Set Method,* Phys. Rev. E, **62, 2,** 2471-2474 (2000)

[13] R.J. LeVeque, *Numerical Methods for Conservations Laws,* Birkhäuser (1992)

[14] J.W.Thomas, *Numerical partial differential equations – Finite difference methods*, Springer (1995)

[15] C.T. Kelley, *Iterative Methods for Linear and Nonlinear Equations,* SIAM (1995)

[16] J. Adam, *General aspects of modeling tumor growth and immune response*, in *A Survey of Models on Tumor Immune Systems Dynamics,* (Edited by J. Adam and N. Bellomo), 15-88, Birkhäuser, Boston, (1997)

[17] J. Folkman, *The Vascularization of Tumors,* Scientific American, May **1976**

[18] H.M. Byrne, L. Preziosi, *Modeling solid tumour growth using the theory of mixtures.* IMA J. Appl. Med. Biol., (2002)

[19] H.M. Byrne, J.R. King, D.L.S. McElwain, L. Preziosi, *A two-phase model of solid tumor growth.* Appl. Math. Letters, (2002)

[20] M. Patra and M. Karttunen, *Stencils with Isotropic Discretization Error for Differential Operators,* online preprint

[21] C.S. Hogea, B.T. Murray and J.A. Sethian, *Simulation of Complex Tumor Evolution in Arbitrary Geometries using a Level Set Method,* in preparation

[22] R.P Araujo and D.L.S. McElwain, *A History of the Study of Tumor Growth: The Contribution of Mathematical Modeling*, 66 (2004) 1039-1091

[23] J.A. Sethian, *Curvature and the Evolution of Fronts,* Comm. in Math.Phys., **101**, 487-499 (1985)

[24] S. Osher and J.A. Sethian, *Fronts Propagating with Curvature-Dependent Speed: Algorithms Based on Hamilton-Jacobi Formulations,* J.Comp.Phys.,**79**, 12-49 (1988)

[25] R. Malladi, J.A. Sethian and B.C. Vemuri, *Shape Modeling with Front Propagation: A Level Set Approach*, IEEE Trans. on Pattern Analysis, **17**, **2**, 158-175 (1995)

Appendix A

Approximation to curvature

In terms of the level set function, the curvature (of the zero level set, as well as of any other level set) is given by

$$\kappa = \nabla \bullet (\frac{\nabla \varphi}{|\nabla \varphi|}) = \frac{\varphi_{xx}\varphi_y^2 - 2\varphi_x\varphi_y\varphi_{xy} + \varphi_{yy}\varphi_x^2}{(\varphi_x^2 + \varphi_y^2)^{\frac{3}{2}}}$$

For the numerical solution procedure, at a grid point (i, j), the corresponding approximation to the curvature $\kappa_{i,j}$ is obtained by using central differencing in all of the above terms.

If the level set function φ remains smooth enough in a neighborhood of the interface, then the curvature at a point on the interface is obtained by bilinear interpolation from the values of the curvature computed at the 4 neighboring nodes on the fixed Cartesian grid (i.e., the 4 corners of the fixed grid cell where the interface point lies).

Approximation to the normal

The local unit outward normal (to the zero level set (i.e., the interface), as well as to all the other level sets) is given by the formula:

$$\vec{n} = \frac{\nabla \varphi}{|\nabla \varphi|} = \frac{(\varphi_x, \varphi_y)}{(\varphi_x^2 + \varphi_y^2)^{\frac{1}{2}}}$$

Here the construction of the approximate normal described in [2] is followed, which takes into account the possibility for the normal to undergo a jump at corners. First, at a grid point (i, j), let:

$$\vec{n}_{i,j}^* := \frac{(D_{i,j}^{+x}, D_{i,j}^{+y})}{\left[(D_{i,j}^{+x})^2 + (D_{i,j}^{+y})^2\right]^{\frac{1}{2}}} + \frac{(D_{i,j}^{-x}, D_{i,j}^{+y})}{\left[(D_{i,j}^{-x})^2 + (D_{i,j}^{+y})^2\right]^{\frac{1}{2}}} + \frac{(D_{i,j}^{+x}, D_{i,j}^{-y})}{\left[(D_{i,j}^{+x})^2 + (D_{i,j}^{-y})^2\right]^{\frac{1}{2}}} + \frac{(D_{i,j}^{-x}, D_{i,j}^{-y})}{\left[(D_{i,j}^{-x})^2 + (D_{i,j}^{-y})^2\right]^{\frac{1}{2}}}$$

where:

$$D_{i,j}^{+x} := \frac{\varphi_{i+1,j} - \varphi_{i,j}}{h} \; , \; D_{i,j}^{-x} := \frac{\varphi_{i,j} - \varphi_{i-1,j}}{h}$$

$$D_{i,j}^{+y} := \frac{\varphi_{i,j+1} - \varphi_{i,j}}{h} \; , \; D_{i,j}^{-y} := \frac{\varphi_{i,j} - \varphi_{i,j-1}}{h}$$

Then the approximate local unit outward normal at the grid point (i, j) is computed as:

$$\vec{n}_{i,j} = \frac{\vec{n}_{i,j}^{*}}{\left| \vec{n}_{i,j}^{*} \right|} \; .$$

Again, as in the case of the curvature, if the level set function φ remains smooth enough in a neighborhood of the interface, then the local unit outward normal at a point on the interface is obtained by bilinear interpolation from the values of the local unit outward normal computed at the four neighboring nodes on the fixed Cartesian grid.

Appendix B

At grid points adjacent to the interface on each side marked as "irregular" in Fig.1, the extension velocity field is constructed by hand. There are two ways of doing this:

I. Let $\vec{x} := (x(i), y(j))$ denote the position of the irregular grid point (i, j) (on either side of the interface); find its projection (i.e. the closest point) on the interface $\vec{x}_{int\,erface}$ by moving along the unit steepest direction:

$$\vec{x}_{int\,erface} = \vec{x} + \alpha \frac{\nabla \varphi(\vec{x}, t)}{\left| \nabla \varphi(\vec{x}, t) \right|} \, ,$$

where α is a real number (positive or negative) to be determined; clearly, $|\alpha| \le h$. Since the level set function on the interface is 0, then:

$$0 = \varphi(\vec{x}_{int\,erface}) = \varphi(\vec{x} + \alpha \frac{\nabla \varphi(\vec{x}, t)}{\left| \nabla \varphi(\vec{x}, t) \right|})$$

and a Taylor series expansion yields:

$$0 = \varphi(\vec{x}, t) + \alpha \left| \nabla \varphi(\vec{x}, t) \right| + \frac{1}{2} \alpha^2 He(\varphi(\vec{x}, t)) \frac{\nabla \varphi(\vec{x}, t)}{\left| \nabla \varphi(\vec{x}, t) \right|} \bullet \frac{\nabla \varphi(\vec{x}, t)}{\left| \nabla \varphi(\vec{x}, t) \right|} + O(\alpha^3)$$

$He(\varphi(\vec{x}, t))$ corresponds to the Hessian matrix of the level set function $\varphi(\vec{x}, t)$. If in the above expansion only the first two terms are kept, then a second order accurate location of the projection on the interface is yielded by $\alpha = -\dfrac{\varphi(\vec{x}, t)}{\left| \nabla \varphi(\vec{x}, t) \right|}$.

If a highly accurate location of the projection is desired, then the first three terms in the above Taylor expansion can be kept and the resulting quadratic algebraic

equation is solved for the unknown α; as long as $\left| \nabla \varphi(\vec{x},t) \right|$ does not depart substantially from 1, the term $He(\varphi(\vec{x},t)) \dfrac{\nabla \varphi(\vec{x},t)}{\left| \nabla \varphi(\vec{x},t) \right|} \bullet \dfrac{\nabla \varphi(\vec{x},t)}{\left| \nabla \varphi(\vec{x},t) \right|}$ remains close to 0, and the discriminant of the quadratic equation for α is safely positive; after solving the equation, the root with the smallest absolute value is picked.

The extension velocity field at the irregular grid point $\vec{x} := (x(i), y(j))$ is obtained by copying the normal velocity of $\vec{x}_{\text{int}erface}$ which is prescribed by Eq. (2.24):

$$F_{i,j} = F_{i,j}(t) = F(\vec{x},t) := F(\vec{x}_{\text{int}erface},t) = V(\vec{x}_{\text{int}erface},t)$$

The advantage of this projection method is its computational efficiency; the potential disadvantage is that if higher order derivatives of the level set function $\varphi(\vec{x},t)$ are involved, this might require usage of the re-initialization procedure more often.

II. A second approach is inspired by the initialization stage of the "Fast Marching Method" described in [2]. While somewhat harder to implement, it has the advantage that it is a purely geometric construction, which does not involve the use of level set function derivatives. Instead, the intersection of the interface with the fixed Cartesian grid lines is required; this is easily obtained from the values of the level set function φ by linear interpolation. The approximate Euclidean distance from the position of an irregular point (i, j) to the front is found purely geometrically, by repeated use of the Pythagorean theorem, depending on the geometrical neighboring configuration; up to a rotation, there are 5 geometrically distinct cases that need to be considered for the neighborhood of an irregular grid point [2]. Thus, the approximate closest point (not found here explicitly) on the interface in this case would lie on a segment of line that is part of the interface reconstructed as a piecewise linear manifold; its normal velocity is obtained by linear interpolation from the values of the normal velocities at the 2 segment ends. As in the previous case, the extension velocity field at the irregular grid point $\vec{x} := (x(i), y(j))$ is obtained by copying the normal velocity of the closest point on the interface.
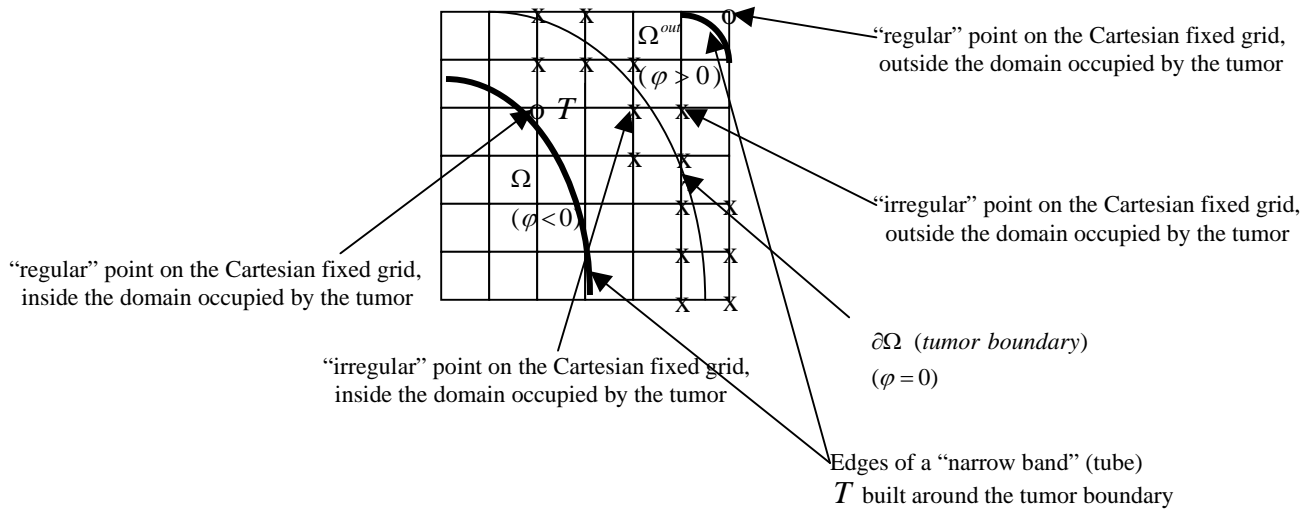
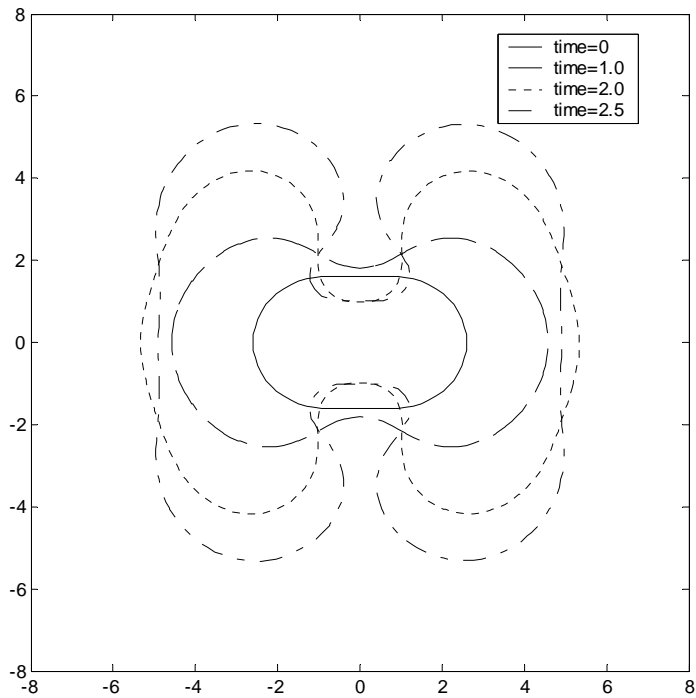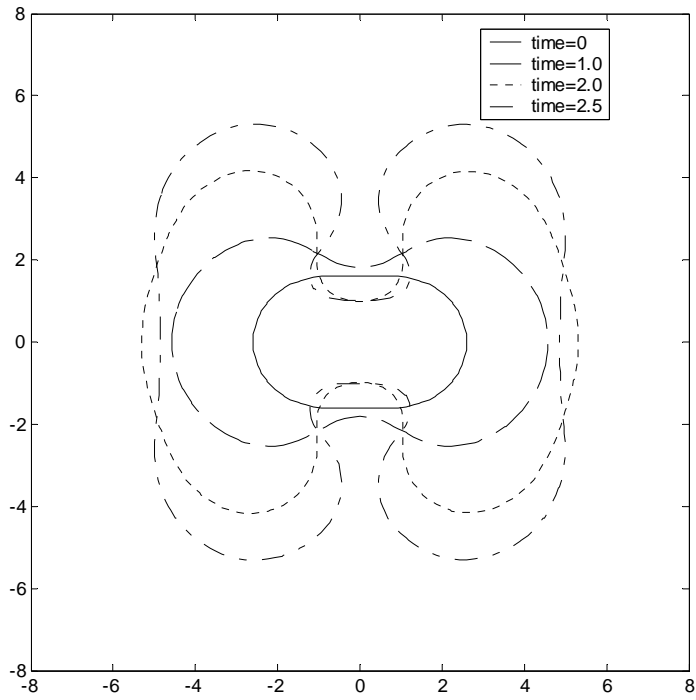**Fig. 1** Schematic of the tumor boundary representation in the Cartesian grid, "narrow band" level set approach.

Fig. 2. Nonlinear tumor evolution in time for unstable growth in the low vascularization regime (G=20, A=0.5): top - full matrix approach WENO used for level set equation; bottom – narrow band approach WENO used for level set equation and re-initialization. Initial tumor boundary given by Eq. (5.1). Mesh size $h = 0.18$ and time step $\Delta t = 0.001$ for both cases.
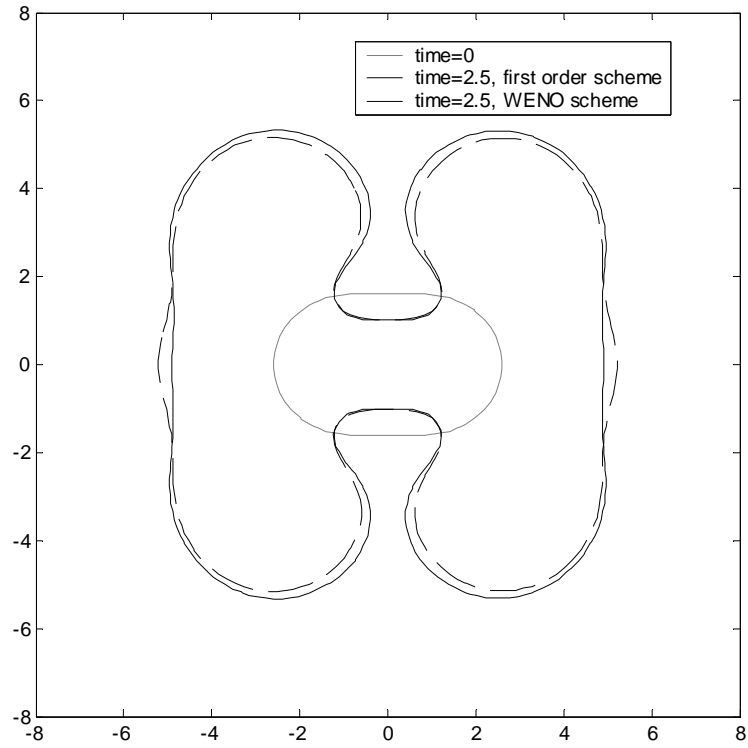
Fig. 3. Comparison of nonlinear tumor evolution in time obtained employing a first-order level set scheme vs. a WENO scheme; the solution obtained via the first-order scheme exhibits numerical dissipation. Initial tumor boundary given by Eq. (5.1), low vascularization regime (G=20, A=0.5). Mesh size $h = 0.18$ and time step $\Delta t = 0.001$.
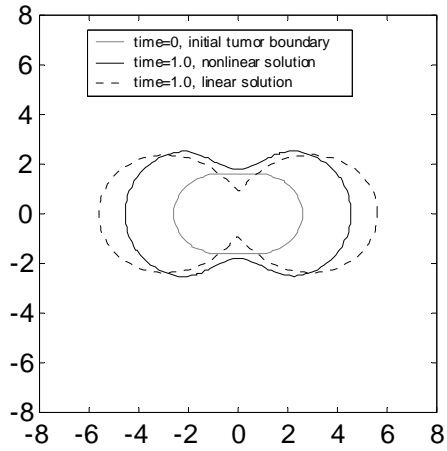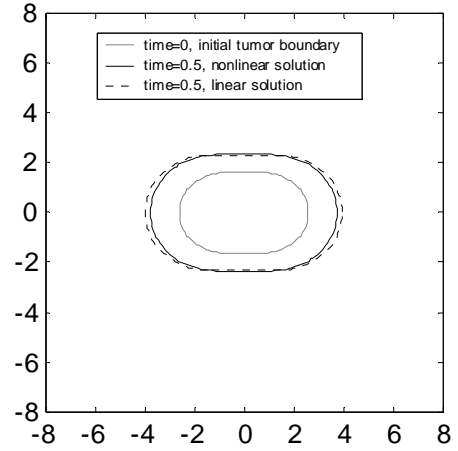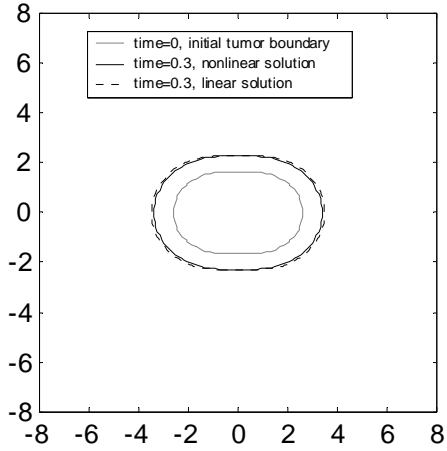
Fig. 4. Comparison between the nonlinear solution obtained via the narrow band level set approach and the solution obtained using the linear analysis developed in [1] for the low vascularization regime (G=20, A=0.5). Initial tumor boundary given by Eq. (5.1). Mesh size $h = 0.18$ and time step $\Delta t = 0.001$.
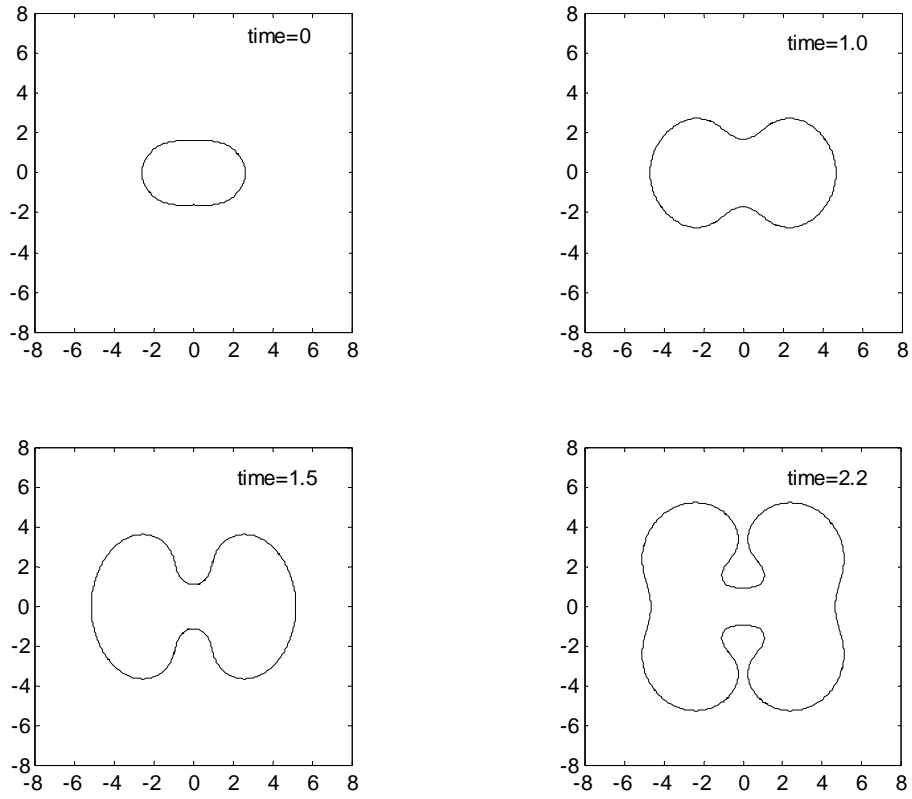
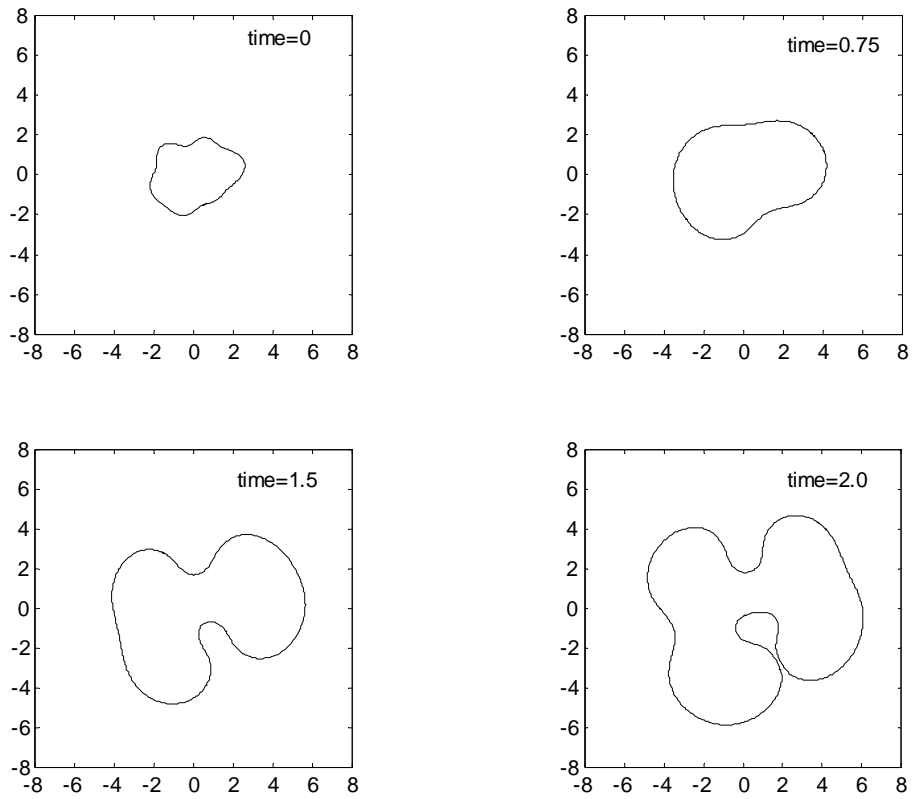**Fig. 5.** Nonlinear tumor evolution in time via the narrow band level set approach (WENO) for the low vascularization regime (G=20, A=0.5). Initial tumor boundary given by Eq. (5.1). Mesh size $h = 0.09$ and time step $\Delta t = 0.00025$.

Fig. 6. Nonlinear tumor evolution in time for the low vascularization regime (G=20, A=0.5) via the narrow band level set approach (WENO scheme). Initial tumor boundary given by Eq. (5.3). Mesh size $h = 0.09$ and time step $\Delta t = 0.00025$.
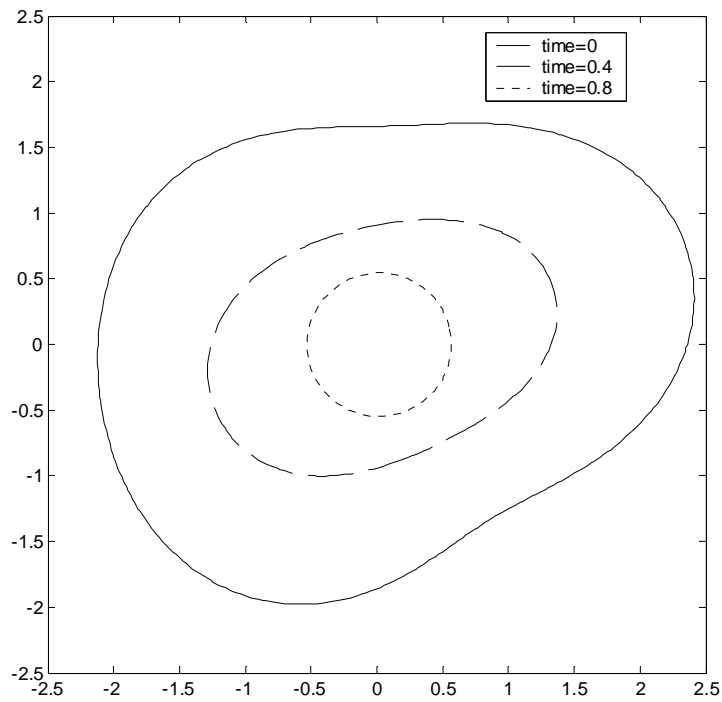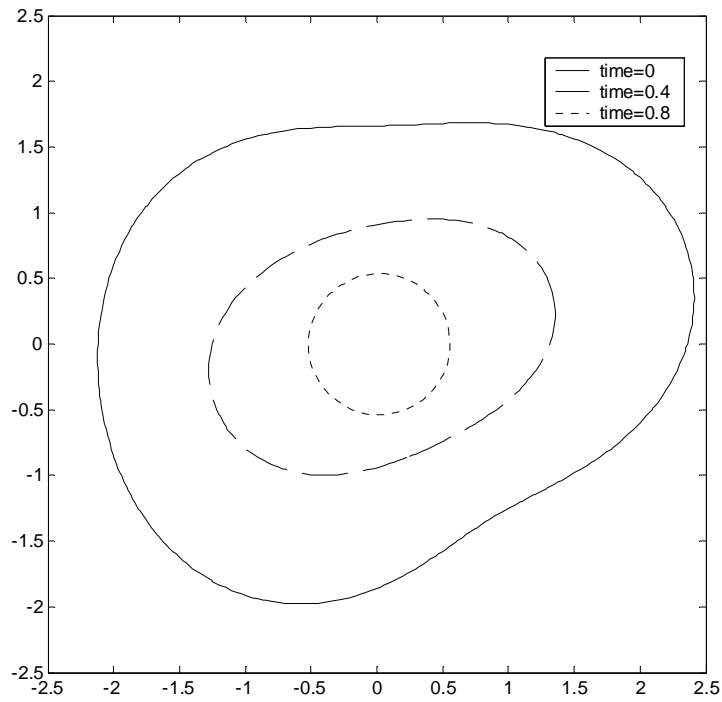
Fig. 7. Nonlinear tumor evolution in time using the narrow band level set approach for parameters in the high vascularization regime (G=-5, A=0.2). Initial tumor boundary shrinks in time. Top: first-order scheme for both the level set and re-initialization; Bottom: WENO scheme used for both. Initial tumor boundary given by Eq. (5.4). Mesh size $h = 0.05$ and time step $\Delta t = 0.00005$.
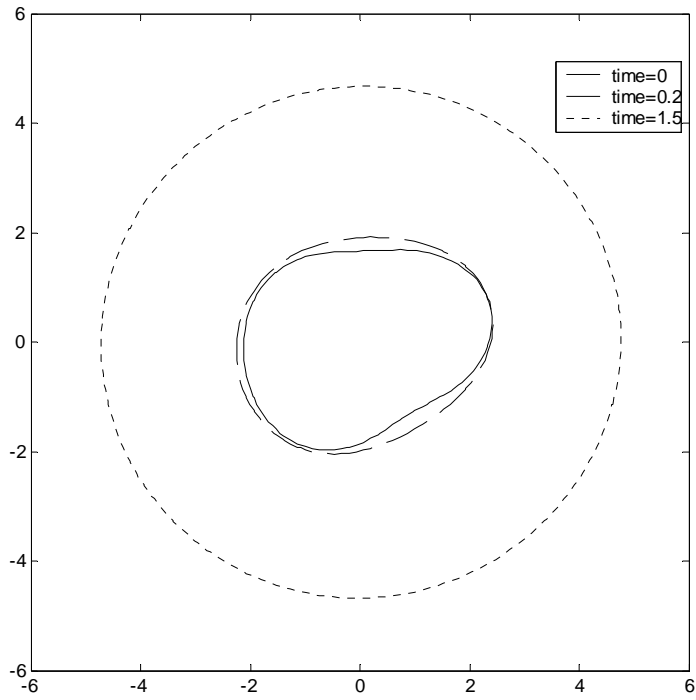
Fig. 8. Nonlinear tumor evolution for unbounded growth obtained via the level set approach in the high vascularization regime (G=-5, A=0.8). Initial tumor boundary given by Eq. (5.4).

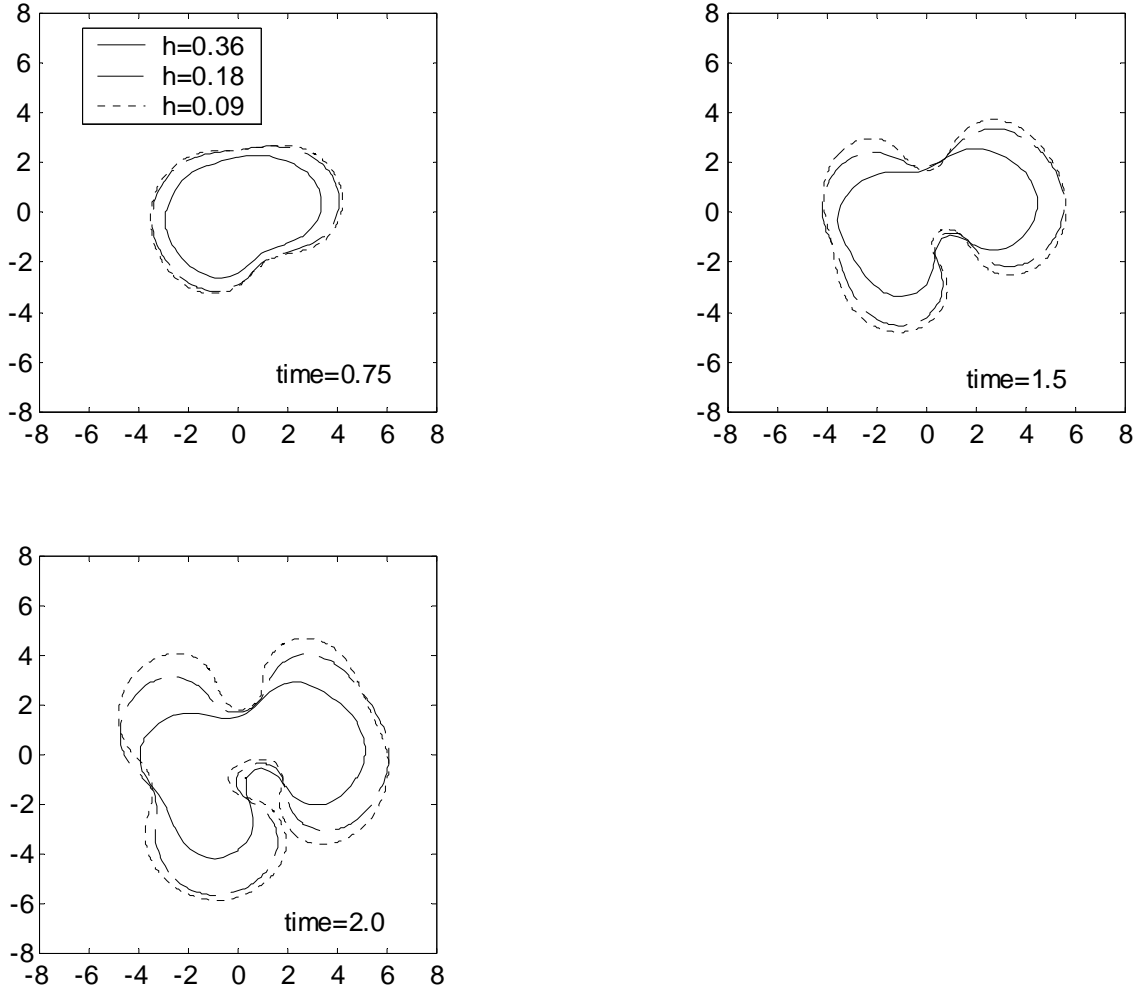**Fig. 9.** Convergence study in the low vascularization regime (G=20, A=0.5). Initial tumor boundary given by Eq. (5.3).

Table 1.

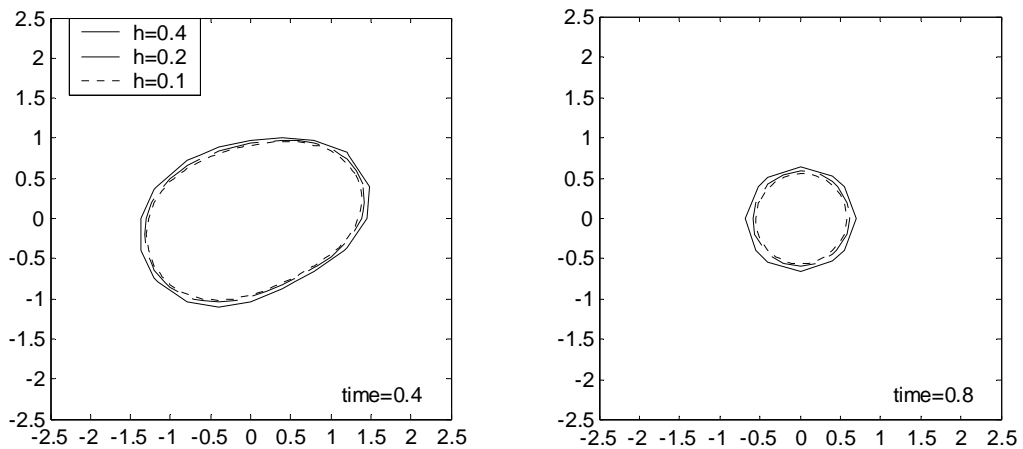| time	$e_{4\_1}^{n}$ (5.5)	$e_{4\_2}^{n}$ (5.6)	$\dfrac{e_{4\_1}^{n}}{e_{4\_2}^{n}}$
t=0.75	0.8725	0.1674	5.2
t=1.5	1.6117	0.5659	2.8747
t=2.0	2.6363	1.2077	2.1827

Fig. 10. Convergence study in the high vascularization regime (G=-5, A=0.2). Initial tumor boundary given by Eq. (5.4).

Table 2.

time	$e^n_{4\_1}$ (5.5)	$e^n_{4\_2}$ (5.6)	$\dfrac{e^n_{4\_1}}{e^n_{4\_2}}$
t=0.4	0.1165	0.0389	2.9961
t=0.8	0.1357	0.0388	3.4927